



CHORUS

This is the accepted manuscript made available via CHORUS. The article has been published as:

Bulk intergrowth of a topological insulator with a room-temperature ferromagnet

Huiwen Ji, J. M. Allred, Ni Ni, Jing Tao, M. Neupane, A. Wray, S. Xu, M. Z. Hasan, and R. J. Cava

Phys. Rev. B **85**, 165313 — Published 19 April 2012

DOI: [10.1103/PhysRevB.85.165313](https://doi.org/10.1103/PhysRevB.85.165313)

Bulk Intergrowth of a Topological Insulator with a Room Temperature Ferromagnet

Huiwen Ji¹, J.M. Allred¹, Ni Ni¹, Jing Tao², M. Neupane³, A. Wray³, S. Xu³, M.Z. Hasan³, and R.J. Cava¹

¹Department of Chemistry, Princeton University, Princeton NJ 08544

²Department of Physics, Brookhaven National Laboratory, Upton NY 11973

³Department of Physics, Princeton University, Princeton NJ 08544

Abstract

We demonstrate that the layered room temperature ferromagnet Fe_7Se_8 and the topological insulator Bi_2Se_3 form crystallographically oriented bulk composite intergrowth crystals. The morphology of the intergrowth in real space and reciprocal space is described. The basal planes of Bi_2Se_3 and Fe_7Se_8 are parallel in the micron-scale intergrowth, and hence the good cleavage inherent to the bulk phases is retained. Both phases in the intergrowth crystals display their intrinsic bulk properties: the ferromagnetism of the Fe_7Se_8 is anisotropic, with magnetization easy axis in the plane of the crystals, and ARPES characterization shows that the topological surface states remain present on the Bi_2Se_3 and that a gap can be observed in the surface state dispersion. Crystals of nominal composition $\text{Bi}_{2-x}\text{Fe}_x\text{Se}_3$ are shown to be bulk intergrowths of the two phases Bi_2Se_3 and Fe_2Se_3 . Significant solubility of Fe in Bi_2Se_3 is not observed.

Introduction

Since the prediction and observation of electronic states with exotic properties on the surfaces of bulk crystals of $\text{Bi}_{1-x}\text{Sb}_x$ [1,2] topological insulators have been of increasing theoretical and experimental interest. Bi_2Se_3 soon emerged as the prototype material for study [3,4] and an increasing body of experimental and theoretical work addresses its properties and potential as a source of new physics and advanced electronic devices. Interactions of the topologically protected surface states with ferromagnetism, although of theoretical interest [e.g. 5-7], have been the subject of little experimental study in bulk crystals [e.g. 8,9], though transition-metal-containing Bi_2Se_3 thin films are emerging [e.g. 10,11]. Here we demonstrate that the layered room temperature ferromagnet Fe_7Se_8 [12] grows very well between layers of Bi_2Se_3 , creating bulk intergrown composite crystals, and that Bi_2Se_3 itself does not dissolve a significant amount of Fe. The ferromagnetism in the intergrown composite $\text{Bi}_2\text{Se}_3:\text{Fe}_7\text{Se}_8$ crystals is anisotropic, with the easy axis for magnetization in-plane, and angle resolved photoemission (ARPES) measurements confirm that the surface states remain present on the Bi_2Se_3 . We postulate that the presence or absence of a gap in the surface state spectra observed in ARPES measurements in the Fe- Bi_2Se_3 system may be due to the proximity of the ARPES excitation spot to the ferromagnetic Fe-Se intergrowth phase in the composite crystals.

Experimental

Composite crystals of $(1-x)\text{Bi}_2\text{Se}_3:x\text{Fe}_7\text{Se}_8$ were grown by the modified Bridgeman method for $x = 0.05, 0.10,$ and 0.20 . Stoichiometric quantities of high purity elemental Bi (99.999%), Se (99.999%), and Fe (99.99%) were used for the $(1-x)\text{Bi}_2\text{Se}_3:x\text{Fe}_7\text{Se}_8$ crystal growth, with nominal x values of 0.05, 0.1, and 0.2. Three-gram mixtures of precleaned elements were sealed in clean quartz ampoules, heated up to $1000\text{ }^\circ\text{C}$ for 3 days followed by cooling to $750\text{ }^\circ\text{C}$. The crystal growth for $(1-x)\text{Bi}_2\text{Se}_3:x\text{Fe}_7\text{Se}_8$ involved cooling from $750\text{ }^\circ\text{C}$ to $620\text{ }^\circ\text{C}$ over a period of 22 h. For $x = 0.05$, such crystals are approximately 10 volume % Fe_7Se_8 , and the larger x values have proportionally more. Visual examination in the optical microscope finds the crystals to have highly lustrous very well defined basal plane cleavage faces for $x = 0.05$, essentially indistinguishable from the surfaces seen in pure Bi_2Se_3 . The cleavage planes become much less well defined and the cleavage surfaces are notably duller by $x = 0.20$. Quantitative analysis of the crystals was first performed by grinding large crystal pieces and performing

powder X-ray diffraction on a Bruker D8 Focus X-ray diffractometer operating with Cu $K\alpha$ radiation and a graphite diffracted beam monochromator, over the angular range $21 \leq 2\theta \leq 38^\circ$ with $\Delta 2\theta = 0.014^\circ$. EDX analysis and SEM images were taken on an FEI Quanta 200 FEG Environmental SEM system. Single crystal X-ray diffraction was performed using a Bruker APEX II using Mo $K\alpha$ radiation ($\lambda = 0.71073 \text{ \AA}$) at 100 K. Exposure time was 30 seconds with a detector distance of 60 mm. Bruker APEX2 software was then utilized to distinguish the reflections of the two phases in the reciprocal space. The orientations of unit cells in the multiple domain crystals were determined using the program CELL_NOW. Pseudoprecession images were assembled digitally from individual frames using the APEX2 software. Specimens for single crystal work were obtained by breaking pieces off of the boule under liquid nitrogen in order to minimize straining the soft crystals. Field-dependent magnetization measurements, $-1 \text{ T} \leq H \leq 5 \text{ T}$, and M vs H measurements at fixed temperatures for $-5 \text{ T} \leq H \leq 5 \text{ T}$, were performed on a Quantum Design Physical Property Measurement System (PPMS). High-resolution angle-resolved photoemission spectroscopy (ARPES) measurements were performed using 15–40 eV photon energies at PGM beamline of the Synchrotron Radiation Centre, Wisconsin and 8–22 eV of photon energies on beamline 5 at the Stanford Synchrotron Radiation Laboratory, California. The energy and momentum resolutions were 15 meV and 2% of the surface Brillouin zone, respectively, obtained using a Scienta R4000 analyzer. The samples were cleaved at 25 K under pressures of less than 5×10^{-11} torr, resulting in shiny flat surfaces. Incident beam spot size was in the range of 30–50 microns.

Results and Discussion

The expanded diffraction patterns for a characteristic angular region are shown in Fig. 1(a). The patterns show the characteristic X-ray fingerprint of Bi_2Se_3 for all samples, with the appearance of lines for Fe_7Se_8 that are weak but clearly discerned in the 0.95:0.05 sample, and which grow substantially by the 0.80:0.20 sample. Thus the $\text{Bi}_2\text{Se}_3:\text{Fe}_7\text{Se}_8$ system is clearly multiple-phase for even low Fe_7Se_8 contents.

The patterns for the powdered crystals do not contain information about the relative orientations of the phases, however, and thus diffraction patterns were obtained for well formed cleaved flat plate crystals of 0.95 Bi_2Se_3 :0.05 Fe_7Se_8 . One of the resulting patterns is shown in Fig. 1 (b). It clearly shows the dominant (00 l) reflections for Bi_2Se_3 (obeying the selection rules

for the rhombohedral space group with $a = 4.143 \text{ \AA}$, $c = 28.636 \text{ \AA}$ [13]) and also shows the (00 l) reflections for Fe_7Se_8 . Fe_7Se_8 is also a layered hexagonal material, though with a different space group and much different lattice parameters (i.e. space group P3_121 , $a = 7.261$ $c = 17.675$ [14]) from Bi_2Se_3 , and is one of the crystallographically ordered compositions in the defect NiAs-type Fe_{1-x}Se solid solution that exists for $0 < x < 0.33$ [15,16]. Thus the diffraction evidence shows that the basal planes of Bi_2Se_3 and Fe_7Se_8 are parallel in the composite intergrowth crystals.

The way that the two phases intergrow in real space is shown in Fig. 2, which is a characterization by scanning electron microscopy (SEM) of a representative portion of a cleaved basal plane surface of one of the intergrown composite crystals. Fig. 2(a) shows the backscattered SEM image for a $\sim 0.04 \text{ mm}^2$ area. Different phases show different degrees of greyness in this image due to the fact that the scattering intensity depends on the atomic number Z . The figure clearly shows that the two different phases intergrow in real space like interlocked fingers. The quantitative chemical analysis of the two phases was performed by energy dispersive X-ray spectroscopy (EDS). Fig. 2(b) shows that the darker area in (a) corresponds quantitatively to the Fe_7Se_8 phase while the lighter area corresponds quantitatively to Bi_2Se_3 . Both phases show excellent basal plane cleavage faces in the SEM images. Fig. 2 (c) shows a side-on view of one of the intergrowth regions. The layered nature of the two phases can clearly be seen, as well as their intergrowth pattern, which is analogous to the stacking of micron-thick cards from two different decks. The Fe_7Se_8 crystal sizes are on the order of 10-100 microns in the large plate dimension and 1-5 microns perpendicular to the plates. The real space phase distribution seen in Figs. 2(a) and (c) is in agreement with the diffraction evidence of Fig. 1: the crystal is indeed an intergrowth of a major Bi_2Se_3 phase with a minor Fe_7Se_8 phase. We imaged approximately 20 pieces of crystals, which all show the intergrowth of the two phases in this fashion, indicating, consistent with Fig. 1(b), that this is the dominant intergrowth pattern: the basal planes of the two layered phases are parallel in the intergrowth, and are therefore structurally and chemically compatible. Further, the EDS analysis did not reveal any solubility of Fe in the bulk Bi_2Se_3 crystals in the composites down to the detectability limit of the EDS method, which is approximately 2%. Thus we conclude that Fe is not soluble to a significant extent in Bi_2Se_3 .

We include in Fig. 2(d) an example of a rarely seen ($< \sim 5\%$) alternative intergrowth geometry for the two phases. In these regions, Bi_2Se_3 grows with its basal plane at a shallow angle on large basal plane oriented crystals of Fe_7Se_8 .

Further detail on the relative orientations of the intergrowth of the Bi_2Se_3 and Fe_7Se_8 phases in the composite crystals was performed by analysis of single crystal X-ray diffraction patterns. As is seen in the real space images, two distinct types of relative crystallographic cell orientations are found in the diffraction space characterization of the intergrowth. The first case, corresponding to the most commonly found orientations in the real space and simple diffraction patterns (Figs. 1(b), 2(a) and 2(c)), is shown in Fig. 2(e), which shows the reciprocal lattice of a composite crystal in the basal plane. In this pattern, the $hk0$ reciprocal lattices (the $[001]$ zones) for both Bi_2Se_3 and Fe_7Se_8 are clearly seen. The reciprocal lattices also have distinct, well defined orientations with respect to each other in the basal $hk0$ plane: the $[100]$ direction of Fe_7Se_8 is parallel to the $[7 -4 0]$ direction of Bi_2Se_3 (a -21° degree in-plane rotation). In matrix form the orientation of Fe_7Se_8 with respect to Bi_2Se_3 is

$$\begin{bmatrix} \cos(21^\circ) & \sin(21^\circ) & 0 \\ -\sin(21^\circ) & \cos(21^\circ) & 0 \\ 0 & 0 & 1 \end{bmatrix}.$$

This pattern indicates that the relative orientations of the Fe_7Se_8 and Bi_2Se_3 domains in the intergrowth is not random, but rather occurs at an optimized orientation that is energetically favorable, i.e. this is a crystallographic intergrowth not a randomly oriented stacking of the two phases. The more complex case corresponding to the shallow-angle intergrowth of the phases shown in real space in Fig. 2(d) is shown in Fig. 2(f). Again, two separate reciprocal lattice planes are observed. One is clearly again the $[001]$ zone of Bi_2Se_3 , i.e. its $hk0$ set of spots. The second is a pseudo-hexagonal set of reflections belonging to the $[111]$ zone of Fe_7Se_8 . This more complex correspondence was identified by collecting a full hemisphere of data (not shown) so the precise orientation of each domain could be determined and compared. The orientation of the Bi_2Se_3 phase with respect to the Fe_{1-x}Se phase is

$$\begin{bmatrix} 0.170 & -0.857 & 0.033 \\ 0.651 & 0.836 & 0.033 \\ -0.834 & 0.140 & 0.175 \end{bmatrix}$$

This corresponds to an out-of-plane canting of approximately 30° , with the in-plane c -axis projection about 10° from the Fe_{1-x}Se [100] direction. The Fe_{1-x}Se reflections are split in all of the measured crystals that exhibit this type of intergrowth. This is evidence that these types of Fe_{1-x}Se domains are nearly but not exactly aligned in each composite crystal. The fact that the orientation differs slightly suggests that the exact optimal interfacial orientation is sensitive to local Fe_{1-x}Se composition; this is not unexpected due to the strong composition dependence of the lattice size of Fe_{1-x}Se .

The physical characterization of the composite $\text{Bi}_2\text{Se}_3:\text{Fe}_7\text{Se}_8$ crystals is summarized in Fig. 3. The two insets shown in the upper left and lower right in Fig. 3(a) show the field-dependent magnetization curves taken at 300 K, 250 K, 200 K, 150 K and 100 K upon zero field cooling (ZFC), on a well formed composite crystal of $0.9\text{Bi}_2\text{Se}_3:0.1\text{Fe}_7\text{Se}_8$ with a regular shape ($3\times 3\times 0.5\text{ mm}^3$). The applied fields are parallel to the c axis, $H//c$, and the ab (basal) plane, $H//ab$, of Bi_2Se_3 for the two insets. Both insets show the presence of strong ferromagnetic character, with the magnetization for $H//ab$ having a quite steep initial slope with applied field, and the magnetization for $H//c$ rising more smoothly, in both cases reaching saturation at relatively low fields. The main panel shows the full hysteresis loops at 100 K for H scans from -5 T to 5 T in both applied field directions. Ferromagnetic hysteresis is clearly seen, and the magnetic behavior is clearly highly anisotropic. Both curves saturate at $\sim 0.25\ \mu_{\text{B}}/\text{Fe}$ atom at 100K, similar to what is observed in pure Fe_7Se_8 [12]. The easy axis, which lies in the ab plane of Fe_7Se_8 , is in the basal plane of Bi_2Se_3 .

Fig. 3(b) shows the characterization by ARPES of the surface states present on the [001] face of a composite $0.95\text{Bi}_2\text{Se}_3:0.05\text{Fe}_7\text{Se}_8$ crystal. The spectra are taken at 25 K, where the ferromagnetism of Fe_7Se_8 is fully developed. Several important characteristics can be observed. Firstly, the surface states remain present on the Bi_2Se_3 part of the composite crystal. The location of the ARPES excitation spot, which is 50-100 microns in size, is not known, so we cannot determine from the current experiments whether the surface states exist on parts of the Bi_2Se_3 near the interface between the Fe_7Se_8 and Bi_2Se_3 intergrown phases where the strongest interactions would occur. The character of the surface states is not significantly different from what is observed in single crystals of Bi_2Se_3 [e.g. 3, 17, 18]. Thirdly, there is substantial density of states in the bulk conduction band of the Bi_2Se_3 , and the composite crystal is an n -type doped

semiconductor, just as is seen in pure native Bi_2Se_3 . Thus the $\text{Bi}_2\text{Se}_3\text{-Fe}_7\text{Se}_8$ composite crystal is ferromagnetic while also displaying topological surface states.

Finally, we show in Fig. 4 that the same coherent two-phase intergrowth phenomena, magnetism, and surface states observed in the $\text{Bi}_2\text{Se}_3\text{:Fe}_7\text{Se}_8$ intergrowth crystals are also observed in bulk crystals that are prepared with the idea that Fe substitution for Bi is possible in bulk Bi_2Se_3 [see e.g. ref. 9]. The SEM secondary electron image of the basal plane cleavage surface of a crystal grown with a nominal formula $\text{Bi}_{1.85}\text{Fe}_{0.15}\text{Se}_3$ is presented in Fig. 4(a). Both phases, the darker Fe_{1-x}Se phase and the lighter Bi_2Se_3 phase, are clearly seen, in analogy to what is seen in Fig. 2(a). Again, EDS measurements show that there is no detectable Fe dissolved in the bulk Bi_2Se_3 . The composition $\text{Bi}_{1.85}\text{Fe}_{0.15}\text{Se}_3$ falls on the two phase $\text{Bi}_2\text{Se}_3\text{-Fe}_2\text{Se}_3$ join (i.e it is 92.5 mol % Bi_2Se_3 : 7.5% mol Fe_2Se_3) and EDS confirms that the Fe_{1-x}Se phase observed has a formula of Fe_2Se_3 . This is the Fe-poor limit of the solid solution phase (i.e. $\text{Fe}_{0.67}\text{Se}$) based on the hexagonal NiAs structure type that is found in the Fe-Se system, which occurs for compositions ranging from 40% Fe (“ Fe_2Se_3 ”) to 50% Fe (FeSe) [15,16]. As is seen for the $\text{Bi}_2\text{Se}_3\text{:Fe}_7\text{Se}_8$ composite crystals, alignment of the basal planes of the Bi_2Se_3 and the Fe_{1-x}Se phases is observed, and both the Bi_2Se_3 and Fe_2Se_3 show excellent cleavage. Fig. 4(b) shows the magnetic characterization of a 0.925 $\text{Bi}_2\text{Se}_3\text{:0.075 Fe}_2\text{Se}_3$ (i.e. “ $\text{Bi}_{1.85}\text{Fe}_{0.15}\text{Se}_3$ ”) intergrown composite crystal. The behavior shadows that seen in Fig. 3(a); the material is ferromagnetic and the magnetization is clearly highly anisotropic, with the easy axis lying in or near the $\text{Bi}_2\text{Se}_3\text{/Fe}_2\text{Se}_3$ basal plane. The background diamagnetism of the undoped Bi_2Se_3 host crystal is clearly seen, especially at the higher fields and higher temperatures for $H//ab$. The ferromagnetism for the Fe_2Se_3 phase in these $\text{Bi}_2\text{Se}_3\text{:Fe}_2\text{Se}_3$ intergrown crystals is weaker than is seen in the $\text{Bi}_2\text{Se}_3\text{:Fe}_7\text{Se}_8$ intergrowths. Further, the ferromagnetism develops significantly only below room temperature. The higher magnification image shown in Fig. 4(a) gives a good view of the typical $\text{Fe}_{1-x}\text{Se}:\text{Bi}_2\text{Se}_3$ interfaces observed in these intergrowth systems. The ARPES data shown in Fig. 4(c) illustrate that the surface states are present in the $\text{Bi}_2\text{Se}_3\text{:Fe}_2\text{Se}_3$ intergrowth crystals just as they are in the $\text{Bi}_2\text{Se}_3\text{:Fe}_7\text{Se}_8$ intergrowth crystals. Comparison of Figs. 3(b) and 4(c) suggests suppression of the spectral weight in the latter spectrum in the vicinity of the Dirac point. Given that the size of the intergrown Fe_{1-x}Se is on the scale of ten to hundreds of microns in the $\text{Bi}_2\text{Se}_3\text{:Fe}_{1-x}\text{Se}$ composite crystals, spectroscopic methods probing the Bi_2Se_3 using relatively small excitation spot sizes (such as ARPES) characterize that compound at varying degrees of

proximity to the ferromagnetic phase depending on the location of the spot; the spectrum shown in 4(c) may be taken from a region of Bi_2Se_3 close to a ferromagnetic intergrowth region of Fe_{1-x}Se , and therefore may show a gap due to physical proximity to the ferromagnetic phase. The same kind of spectra may also be observed in the $\text{Bi}_2\text{Se}_3:\text{Fe}_7\text{Se}_8$ composite crystals.

Conclusion

In conclusion we have demonstrated that the room temperature ferromagnet Fe_7Se_8 is chemically and structurally compatible with the topological insulator Bi_2Se_3 to such a great extent that the two phases intergrow in crystallographically oriented micron thick layers in bulk crystals. The phases exhibit their intrinsic bulk properties; the ferromagnetism and the topological surface states are present in the composite crystals. Our results suggest that multilayer ferromagnetic Fe_7Se_8 – topological insulator Bi_2Se_3 thin films can likely be grown with crystallographically coherent interfaces. The surfaces of cleaved $\text{Fe}_7\text{Se}_8:\text{Bi}_2\text{Se}_3$ (or $\text{Bi}_{2-x}\text{Fe}_x\text{Se}_3$) composite crystals offer the opportunity for exploring the interactions between topological surface states and ferromagnetism if care is taken to attend to the inhomogeneous distribution of the constituent phases.

Acknowledgements

The crystal growth and ARPES characterization were supported by NSF grant DMR-0819860, the single crystal diffraction by NSF grant DMR-1005438, and the magnetic and microscopic characterization by DARPA grant SPAWAR N66001-11-1-4110. The work at BNL was supported by the U.S. Department of Energy (Basic Energy Sciences) and by the Materials Science and Engineering Division under Contract No. DE-AC02-98CH10886 and through the use of the CFN. RC acknowledges fruitful discussions with G. Panaccione and A. Yazdani.

Figures

Fig. 1 (Color on line) Characterization of the $\text{Bi}_2\text{Se}_3:\text{Fe}_7\text{Se}_8$ intergrowth crystals by large-scale diffraction methods. (a) Characteristic region of powder X-ray diffraction patterns for ground crystals grown for different Fe_7Se_8 concentrations $(1-x)\text{Bi}_2\text{Se}_3:x\text{Fe}_7\text{Se}_8$. The primary pattern is from Bi_2Se_3 , whose expected Bragg peak positions are marked with ticks. The second phase Fe_7Se_8 peaks grow in intensity with increasing x . (b) The diffraction pattern from the cleaved basal plane crystal surface of a 3mm x 3mm $0.9\text{Bi}_2\text{Se}_3:0.1\text{Fe}_7\text{Se}_8$ intergrowth crystal. Clearly observed are the $00l$ reflections from Bi_2Se_3 , which obey the rhombohedral diffraction condition $l=3n$, and the $00l$ reflections from Fe_7Se_8 . This shows that the basal planes of the two phases in the intergrowth crystals are aligned.

Fig. 2 (color on line) Real space and reciprocal space characterization of the intergrowth crystals. (a) backscattered electron image on the cleaved basal plane surface of an $0.95\text{Bi}_2\text{Se}_3:0.05\text{Fe}_7\text{Se}_8$ intergrowth crystal showing the distribution of the Fe_7Se_8 phase (dark areas) and the Bi_2Se_3 phase (light area). The intergrowth of basal plane regions occurs at the tens of microns length scale. (b) The associated EDS data that identifies the two regions in (a) as Fe_7Se_8 (dark regions) and Bi_2Se_3 (light regions). No detectable Fe can be found in the Bi_2Se_3 regions. (c) A side-on view of an intergrowth crystal showing that the intergrowth occurs on the micron scale in the direction perpendicular to the cleavage plane. (d) A much rarer but also occasionally encountered shallow angle growth of Bi_2Se_3 on the basal plane of Fe_7Se_8 . Reciprocal space planes of intergrowth crystals obtained by single crystal X-ray diffraction are shown in panels (e) and (f). These reciprocal space planes are in the planes of the physical crystal plates. The reciprocal lattices for Bi_2Se_3 are marked by white lines and of Fe_7Se_8 are marked by green lines.

Fig. 3 (color on line) Magnetic and ARPES characterization of $0.95\text{Bi}_2\text{Se}_3:0.05\text{Fe}_7\text{Se}_8$ intergrowth crystals. The insets to panel (a) show that the crystal is ferromagnetic at room temperature, and that the saturation magnetization grows with decreasing temperature. The main panel in (a) shows the development of the magnetization with applied field at 100 K for the crystal aligned with the magnetic field perpendicular to the plate ($H//c$) and the magnetic field in the plane of the plate ($H//ab$). The easy axis of the magnetization is in the basal plane. (b and c) High resolution ARPES spectra along the high symmetry $M-\Gamma-M$ direction showing that the topological surface states are clearly present on the intergrowth crystals at 25 K. The photon energy employed in the measurement is noted; the Fermi energy is at $E=0$; the bulk conduction

band (BCB) is seen for $E > \sim -0.2$ eV and the bulk valence band (BVB) for $E < \sim -0.5$ eV. The surface state (SS) bands are the fine features between the top of the BVB and the bottom of the BCB.

Fig. 4 (color on line) Real space, magnetic, and ARPES characterization of bulk “single crystals” of “ $\text{Bi}_{1.85}\text{Fe}_{0.15}\text{Se}_3$ ”. As in the $(1-x)\text{Bi}_2\text{Se}_3:x\text{Fe}_7\text{Se}_8$ case, these crystals are again two phase intergrowths, actually described as the intergrowth composite $0.925\text{Bi}_2\text{Se}_3:0.075\text{Fe}_2\text{Se}_3$. (a) The real space intergrowth of the two phases on a basal plane crystal cleavage surface. The Fe_{1-x}Se phase has the formula Fe_2Se_3 , determined by EDS, and is shown as the dark phase in the secondary electron image. EDS analysis shows that there is no Fe present in the Bi_2Se_3 (the lighter phase in the image) (b) The magnetic characterization of a $0.925\text{Bi}_2\text{Se}_3:0.075\text{Fe}_2\text{Se}_3$ (i.e. “ $\text{Bi}_{1.85}\text{Fe}_{0.15}\text{Se}_3$ ”) crystal, showing weaker ferromagnetism than in the $\text{Bi}_2\text{Se}_3:\text{Fe}_7\text{Se}_8$ intergrowth crystals, developing at lower temperature. At high fields the intrinsic diamagnetism of the Bi_2Se_3 is clearly seen in both field directions. The easy axis of the magnetization is in the basal plane. (c) High resolution ARPES characterization of one of the “ $\text{Bi}_{1.85}\text{Fe}_{0.15}\text{Se}_3$ ” composite intergrowth crystals along the high symmetry $\text{M}-\Gamma-\text{M}$ direction showing that the topological surface states are clearly present on the intergrowth crystals at 25 K. The photon energy employed in the measurement is noted; the Fermi energy is at $E=0$; the bulk conduction band (BCB) is seen for $E > \sim -0.05$ eV and the bulk valence band (BVB) for $E < \sim -0.4$ eV. The surface state (SS) bands are the fine features between the top of the BVB and the bottom of the BCB.

References

- [1]. L. Fu, C.L. Kane, and E.J. Mele, *Phys. Rev. Lett.* **98**, 106803 (2007).
- [2]. D. Hsieh, D. Qian, L. Wray, Y. Xia, Y. S. Hor, R. J. Cava, and M. Z. Hasan, *Nature* **452**, 970 (2008).
- [3]. Y. Xia, D. Qian, D. Hsieh, L. Wray, A. Pal, A. Bansil, D. Grauer, Y. S. Hor, R. J. Cava, and M. Z. Hasan, *Nature Phys.* **5**, 398 (2009).
- [4] H.-J. Zhang, C-X Liu, X-L Qi, X. Dai, Z. Fang and S.-C. Zhang, *Nature Phys.* **5**, 438 (2009).
- [5] Rui Yu, Wei Zhang, Hai-Jun Zhang, Shou-Cheng Zhang, Xi Dai, Zhong Fang, H.-J. Zhang, X. Zhang and S.-C. Zhang, *Science* **329**, 61 (2010).
- [6] Gil Young Cho and Joel E. Moore, *Phys. Rev. B* **84**, 165101 (2011).
- [7] Hosub Jin, Jung-Hwan Song, and Arthur J. Freeman, *Phys. Rev. B* **83** 125319 (2011).
- [8] Haim Beidenkopf, Pedram Roushan, Jungpil Seo, Lindsay Gorman, Ilya Drozdov, Yew San Hor, R. J. Cava and Ali Yazdani, *Nature Phys.* **7** 939 (2011).
- [9] Y. L. Chen, J.-H. Chu, J. G. Analytis, Z. K. Liu, K. Igarashi, H.-H. Kuo, X. L. Qi, S. K. Mo, R. G. Moore, D. H. Lu, M. Hashimoto, T. Sasagawa, S. C. Zhang, I. R. Fisher, Z. Hussain, Z. X. Shen, *Science* **329**, 659 (2010).
- [10] P. P. J. Haazen, J.-B. Laloe, T. J. Nummy, H. J. M. Swagten, P. Jarillo-Herrero, D. Heiman, and J. S. Moodera, *Appl. Phys. Lett.* **100**, 082404 (2012).
- [11] Minhao Liu, Jinsong Zhang, Cui-Zu Chang, Zuocheng Zhang, Xiao Feng, Kang Li, Ke He, Li-li Wang, Xi Chen, Xi Dai, Zhong Fang, Qi-Kun Xue, Xucun Ma, and Yayu Wang, *Phys. Rev. Lett.* **108** 036805 (2012).
- [12] T. Kamimura, K. Kamigaki, T. Hirone, and K. Sato, *J. Phys. Soc. Jpn.* **22** 1235 (1967).
- [13] S. Nakajima, *J. Phys. Chem. Sol.* **24** 479 (1963).
- [14] J.B. Parise, A. Nakano, M. Tokonami, and N. Morimoto, *Acta Crystallographica B* **35** 1210 (1979).
- [15] J.E. Dutrizac, M.B.I. Janjua, and J.M. Toguri, *Can. J. Chem.* **46** 1171 (1968).
- [16] W. Schuster, H. Mikler, and K. L. Komarek, *Monatshfte fur Chemie* **110**, 1153 (1979).
- [17] Y.S. Hor, A. Richardella, P. Roushan, Y. Xia, J.G. Checkelsky, A. Yazdani, M.Z. Hasan, N.P. Ong, and R.J. Cava, *Phys. Rev. B* **79** 195208 (2009).
- [18] Z.H. Pan, E. Vescovo, A.V. Fedorov, D. Gardner, Y.S. Lee, S. Chu, G.D. Gu, and T. Valla, *Phys. Rev. Lett.* **106** 257004 (2011).

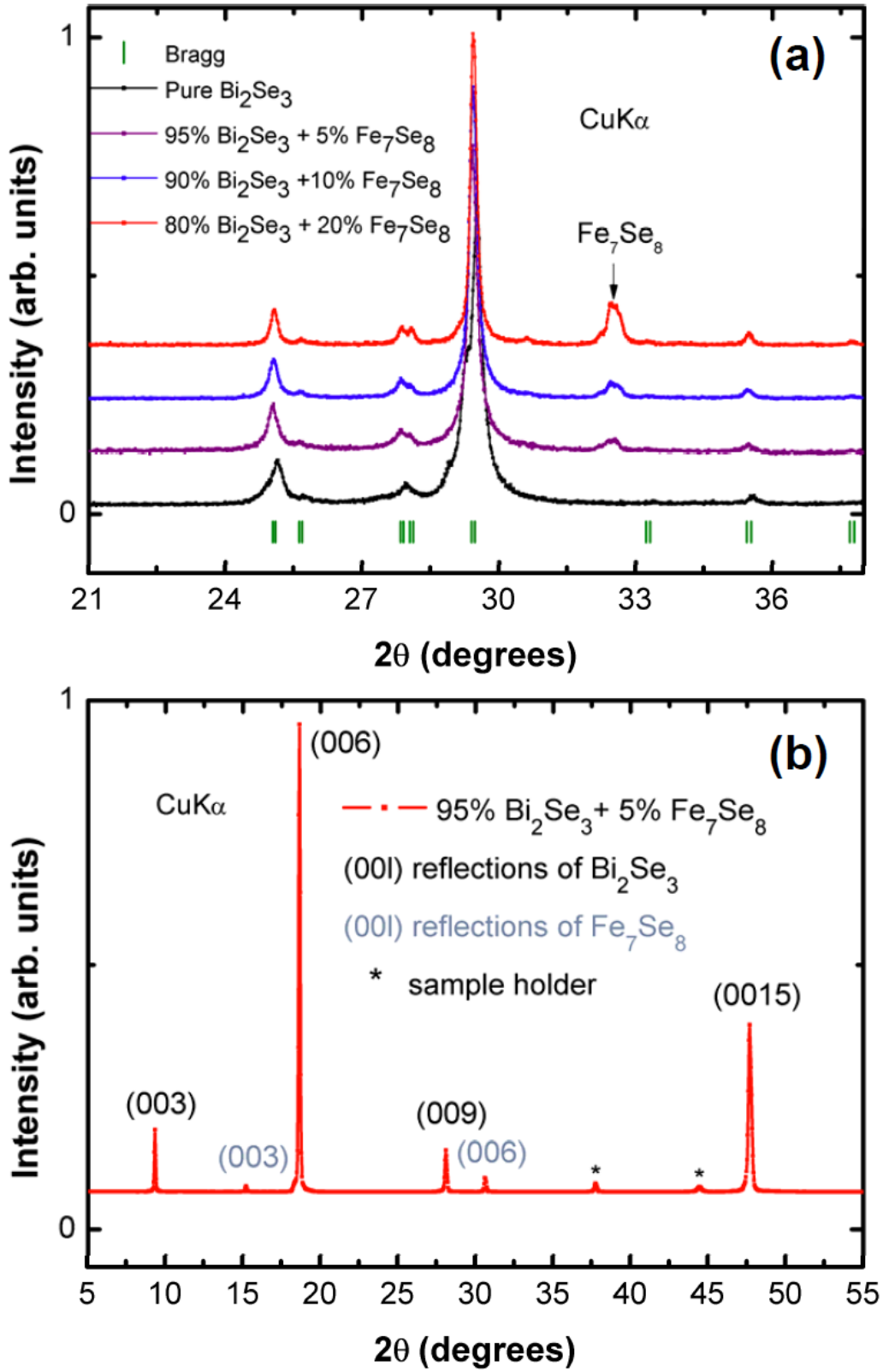


Figure 1

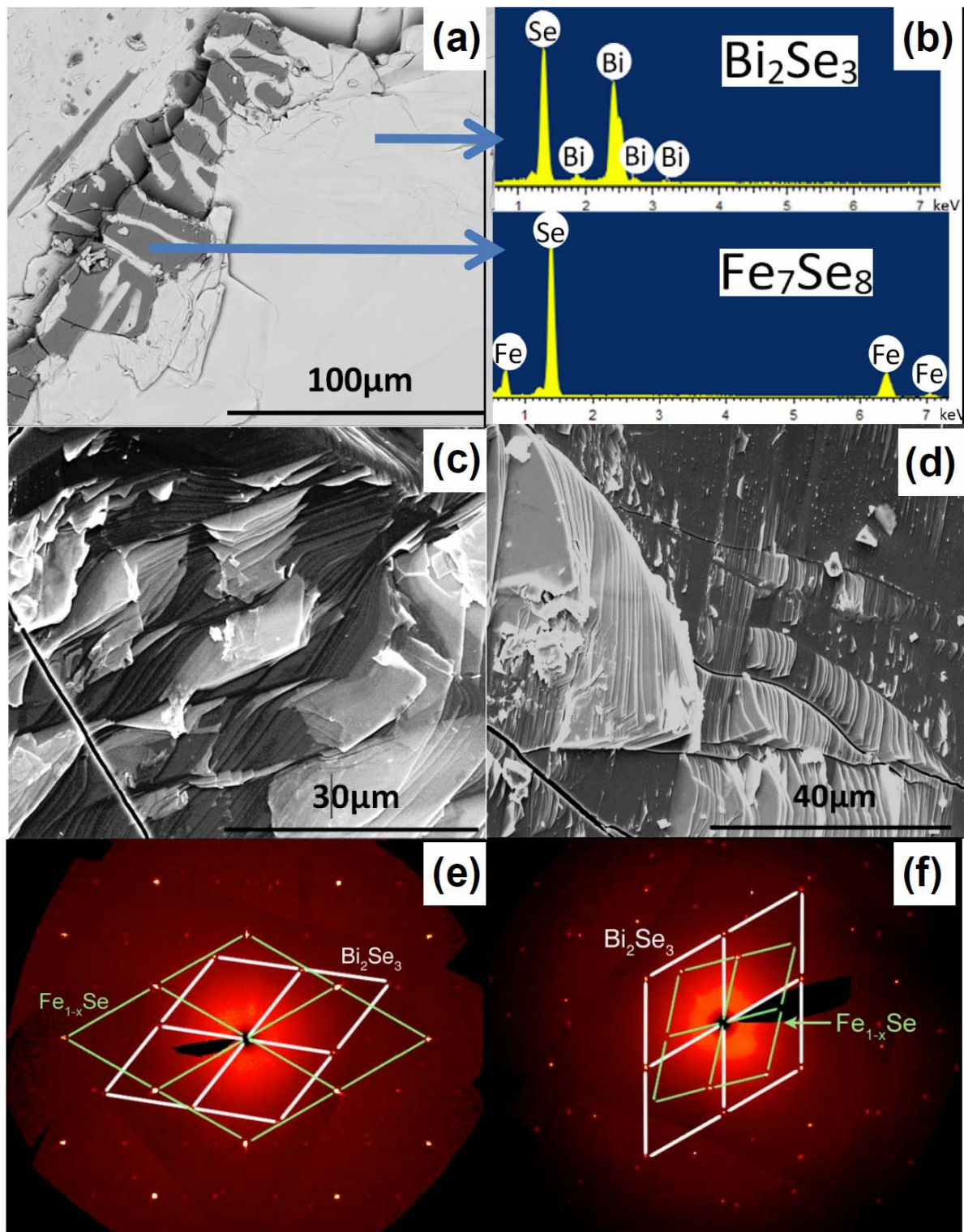


Figure 2

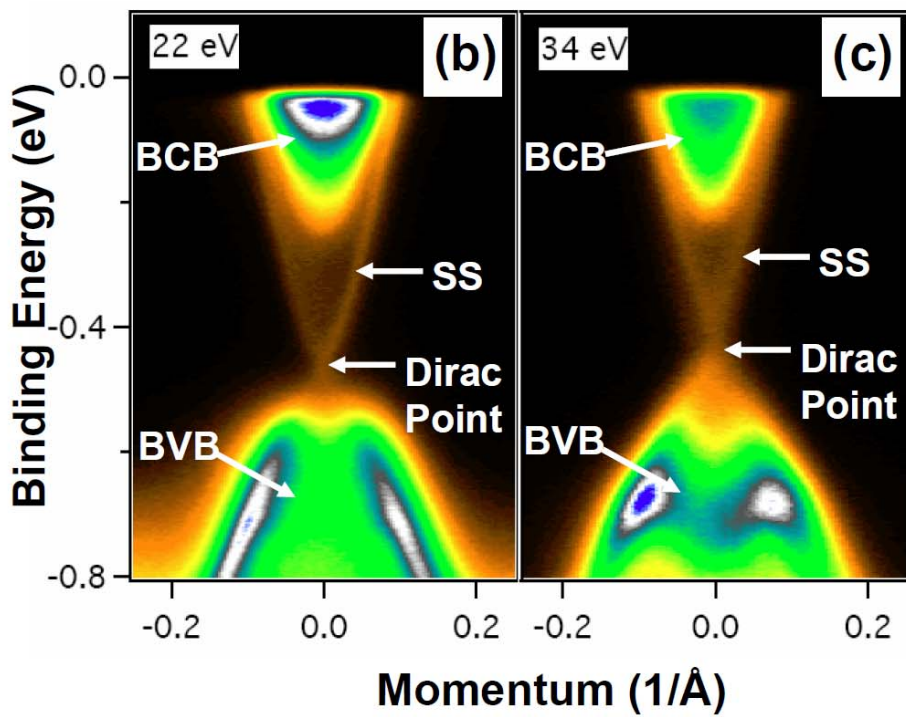
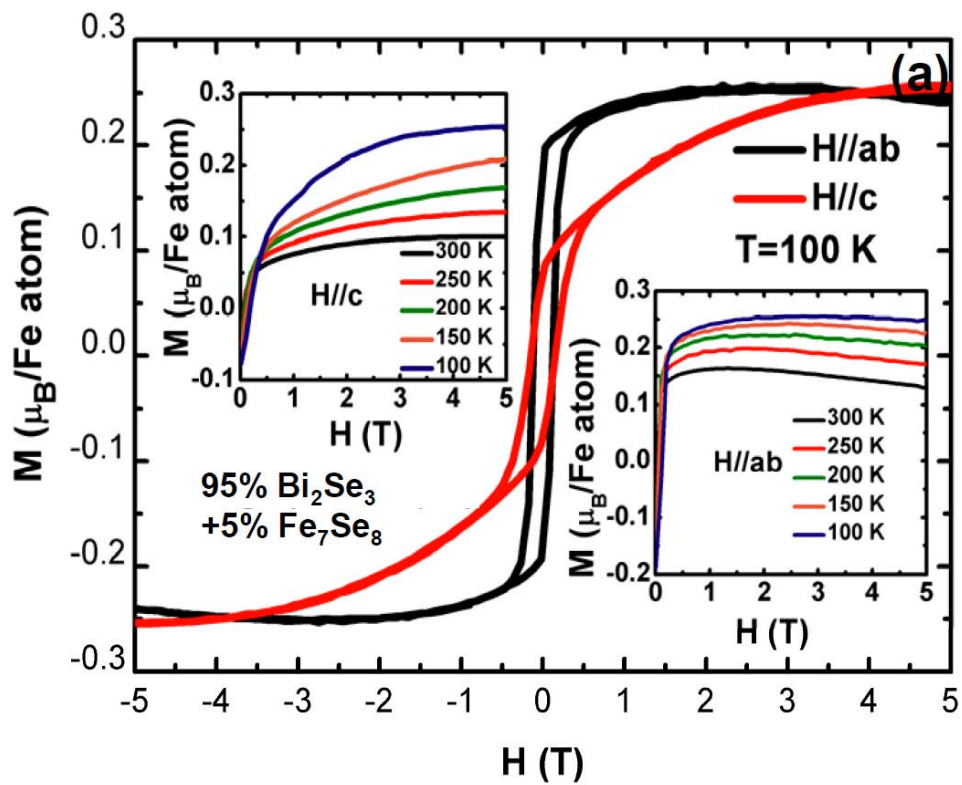


Figure 3

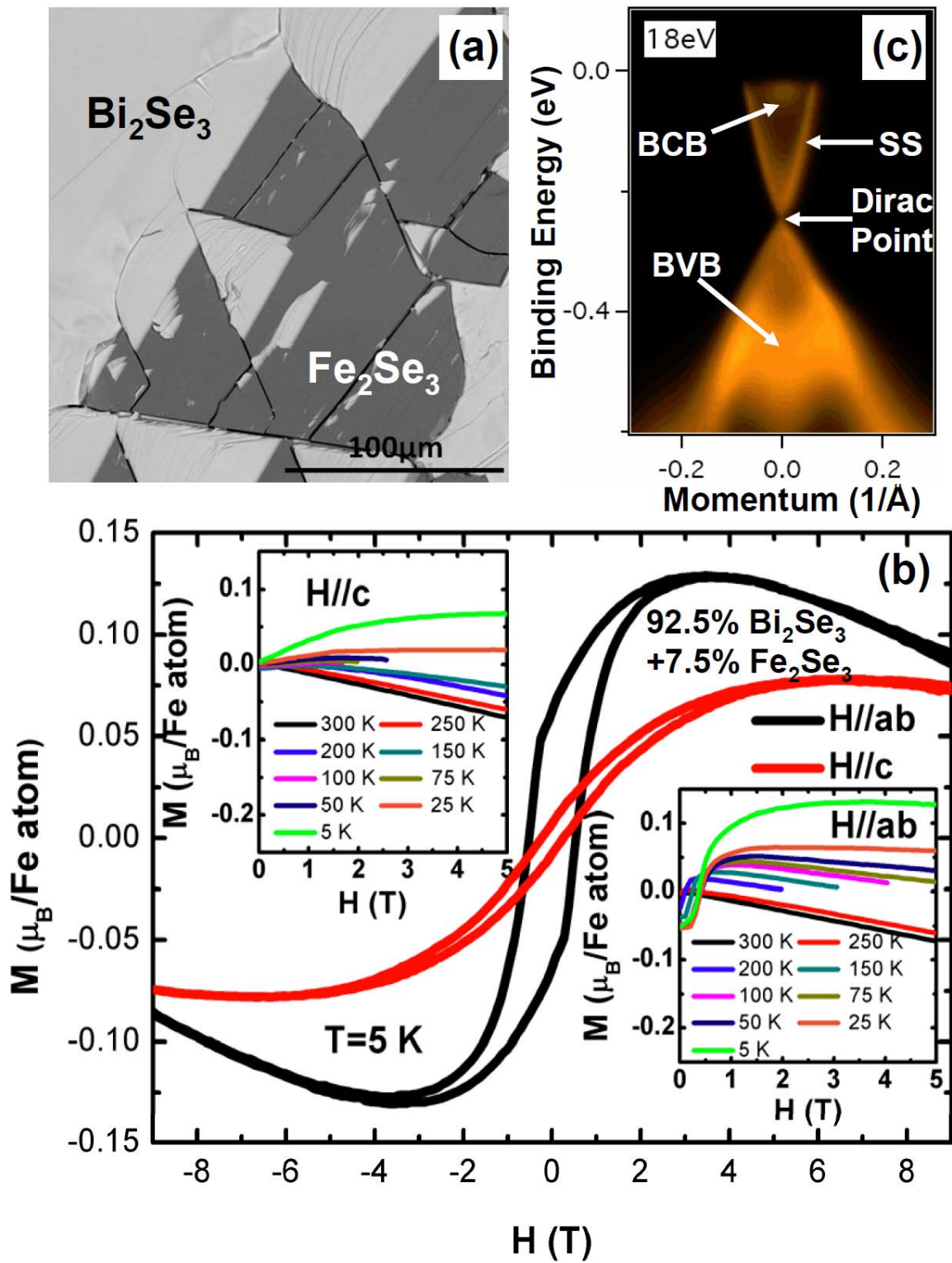


Figure 4